J. Fluid Mech. (2017), *vol.* 813, R1, doi:10.1017/jfm.2017.1

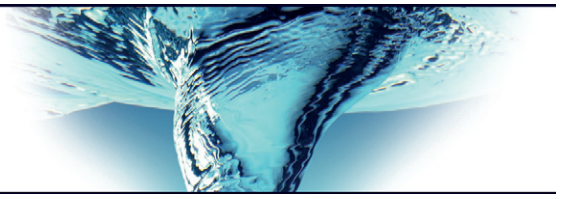

JFM RAPIDS
journals.cambridge.org/rapids

Asymptotic solution for high-vorticity regions in incompressible three-dimensional Euler equations

D. S. Agafontsev[1,2], E. A. Kuznetsov[2,3] and A. A. Mailybaev[4,†]

[1]P. P. Shirshov Institute of Oceanology, Moscow 117218, Russia

[2]Novosibirsk State University, Novosibirsk 630090, Russia

[3]P. N. Lebedev Physical Institute, Moscow 119991, Russia

[4]Instituto Nacional de Matemática Pura e Aplicada – IMPA, Rio de Janeiro 22460-320, Brazil

(Received 25 September 2016; revised 23 December 2016; accepted 23 December 2016; first published online 17 January 2017)

Incompressible three-dimensional Euler equations develop high vorticity in very thin pancake-like regions from generic large-scale initial conditions. In this work, we propose an exact solution of the Euler equations for the asymptotic pancake evolution. This solution combines a shear flow aligned with an asymmetric straining flow, and is characterized by a single asymmetry parameter and an arbitrary transversal vorticity profile. The analysis is based on detailed comparison with numerical simulations performed using a pseudospectral method in anisotropic grids of up to $972 \times 2048 \times 4096$.

Key words: vortex dynamics, vortex flows

1. Introduction

The mechanism of vorticity growth in the incompressible three-dimensional (3D) Euler equations, in the absence of a physical boundary, has been addressed in numerous studies because of its relation to a possible finite-time blowup and subsequent transition to turbulence. Several analytical blowup and no-blowup criteria have been established; see the reviews in Chae (2008) and Gibbon (2008). In parallel, a large amount of effort has been made with numerical analysis. In one of the early numerical studies, Brachet *et al.* (1992) examined the evolution of periodic flows in 256^3 grids for random initial conditions and in 864^3 grids for the symmetric Taylor–Green vortex. In all cases, the maximum of vorticity grew nearly exponentially with time, and the regions of high vorticity were confined within pancake-like structures (thin vortex sheets). An exact solution of the Euler equations

† Email address for correspondence: alexei@impa.br

was suggested as a model for asymptotic pancake development, with the relation $\omega_{max}(t) \propto 1/\ell(t)$ between the vorticity maximum and the pancake thickness. Since the tendency towards a vortex sheet should suppress three-dimensionality of the flow, formation of a finite-time singularity is not expected. It should be recalled that the dynamics of the two-dimensional (2D) Euler equations is known to be regular; see Majda & Bertozzi (2002) and the related discussion in Pumir & Siggia (1990) and Ohkitani (2008). Thus, further numerical studies were mainly concentrated on carefully designed initial conditions providing enhanced vorticity growth. We refer to Gibbon (2008) and Agafontsev, Kuznetsov & Mailybaev (2015) for a brief review, as well as to Hou (2009), Bustamante & Brachet (2012) and Kerr (2013) for examples of recent numerical works. It is fair to say that we do not possess sufficiently reliable evidence supporting the blowup hypothesis yet.

In our previous study, see Agafontsev *et al.* (2015), we returned to the problem of vorticity growth from generic large-scale initial conditions and focused on numerical description of flow details with high resolution. Two simulations were carried out with grids of up to $486 \times 1024 \times 2048$ and $1152 \times 384 \times 2304$ for initial conditions designated as I_1 and I_2. Self-similar development of the pancake-like regions of high vorticity was observed. However, significantly different exponents ($\beta_2/\beta_1 \approx 2/3$) were measured for the maximum vorticity growth $\omega_{max}(t) \propto \mathrm{e}^{\beta_2 t}$ and the pancake compression in the transversal direction $\ell(t) \propto \mathrm{e}^{-\beta_1 t}$, demonstrating that the pancake model with $\omega_{max}(t) \propto 1/\ell(t)$ suggested in Brachet *et al.* (1992) is insufficient. Pancake structures emerged in increasing number with time. These structures provided the leading contribution to the energy spectrum, where we observed the gradual formation of the Kolmogorov spectrum, $E(k) \propto k^{-5/3}$, in a fully inviscid flow.

In the present paper, we demonstrate that the asymptotic pancake evolution can be described by a new exact solution of the Euler equations, which combines a shear flow aligned with an asymmetric straining flow. This solution represents an essential generalization of the pancake model of Brachet *et al.* (1992) and agrees with the numerical data. We illustrate our results with the simulation with the I_1 initial condition from Agafontsev *et al.* (2015), performed here in an eight times larger grid of up to $972 \times 2048 \times 4096$, and concentrate our analysis on the main pancake structure containing the global vorticity maximum. We checked that other pancake structures, as well as pancakes developing in simulations with different initial conditions, also agree with the exact solution.

The paper is organized as follows. Section 2 describes the numerical method and demonstrates general properties of a pancake structure. The exact solution of the 3D Euler equations is proposed in § 3 as a model for asymptotic pancake evolution. In § 4, we provide several numerical tests comparing the analytical model with the simulations. The final section contains conclusions.

2. Pancake vorticity structures

We analyse the evolution of high-vorticity regions with numerical simulations of the Euler equations (in the vorticity formulation),

$$\frac{\partial \boldsymbol{\omega}}{\partial t} = \mathrm{rot}\,(\boldsymbol{v} \times \boldsymbol{\omega}), \quad \boldsymbol{v} = \mathrm{rot}^{-1}\boldsymbol{\omega}, \tag{2.1}$$

in the periodic box $\boldsymbol{r} = (x, y, z) \in [-\pi, \pi]^3$. The pseudospectral Runge–Kutta fourth-order method is used, together with the Fourier cutoff function suggested in Hou & Li (2007) to avoid the bottle-neck instability. The inverse of the curl operator and all

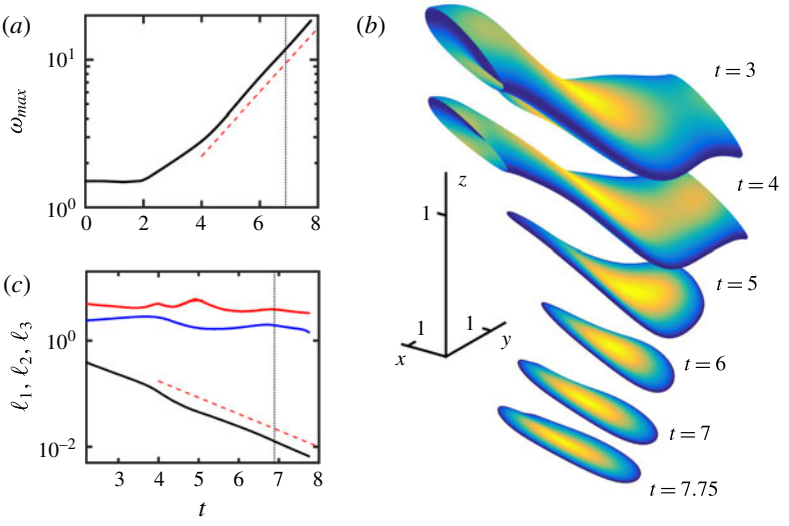

FIGURE 1. (*a*) Global vorticity maximum as a function of time (logarithmic vertical scale). The red dashed line indicates the slope $\propto e^{\beta_2 t}$, with $\beta_2 = 0.5$. The thin vertical line marks the final simulation time $t = 6.89$ in Agafontsev *et al.* (2015). (*b*) Regions of the largest vorticity, $\omega \geqslant 0.85\omega_{max}(t)$, at different times. The colour represents the vorticity in the midplane of the pancake, from blue for $0.85\omega_{max}(t)$ to yellow for $\omega_{max}(t)$. The structures are shifted vertically for better visualization. (*c*) Characteristic spatial scales ℓ_1 (black), ℓ_2 (blue) and ℓ_3 (red) of the pancake structure. The red dashed line indicates the slope $\propto e^{-\beta_1 t}$, with $\beta_1 = 0.74$.

spatial derivatives are calculated in the Fourier space. We start from initial condition I_1 of Agafontsev *et al.* (2015), which represents a perturbation of the shear flow $\omega_x = \sin z$, $\omega_y = \cos z$, $\omega_z = 0$. Taking advantage of the anisotropy of the vorticity field, we use an adaptive anisotropic rectangular grid, which is uniform along each direction and adapted independently along each coordinate. For more details of the numerical scheme, see Agafontsev *et al.* (2015), where it was verified that the accuracy within the simulation time interval is very high and is not affected by the Fourier cutoff filter. The simulation previously stopped at time $t = 6.89$ with the grid $486 \times 1024 \times 2048$ is continued here until $t = 7.75$ with the eight times larger final grid $972 \times 2048 \times 4096$, when the thinnest pancake structure is resolved with 10 grid points at the level of vorticity half-maximum. The results of the two simulations converge perfectly at the same times. Both the energy $E = (1/2)\int \boldsymbol{v}^2 \, \mathrm{d}^3\boldsymbol{r}$ and the helicity $\Omega = \int (\boldsymbol{v} \cdot \boldsymbol{\omega}) \, \mathrm{d}^3\boldsymbol{r}$ are conserved, with a relative error smaller than 10^{-11}.

Figure 1(*a*) shows the evolution of the global vorticity maximum $\omega_{max}(t) = \max_{\boldsymbol{r}} |\boldsymbol{\omega}(\boldsymbol{r}, t)|$, demonstrating the vorticity increase from $\omega_{max}(0) = 1.5$ up to 18.4 at $t = 7.75$ and the asymptotically exponential vorticity growth at late times. Figure 1(*b*) shows the three-dimensional regions containing the vorticity $\omega = |\boldsymbol{\omega}| \geqslant 0.85\omega_{max}(t)$ at different times, and one can clearly see the formation of a thin pancake structure. It is convenient to introduce the pancake midplane as a surface, where the vorticity attains a maximum within the pancake thickness. The colour in figure 1(*b*) describes the midplane vorticity, from blue for $0.85\omega_{max}(t)$ to yellow for $\omega_{max}(t)$. At $t = 3$ and 4, the pancake spans the whole periodic domain in the x-direction; for larger times, its lateral sizes decrease, but eventually stabilize and remain almost constant at $t \geqslant 6$.

On the contrary, the thickness keeps decreasing rapidly. Thus, at late times, vorticity variations become large (small) in transversal (tangential) directions to the pancake.

The local geometry of the thin structure can be studied using the Hessian matrix $\partial_i\partial_j\omega^2$ of second derivatives of ω^2 with respect to (x, y, z), computed at the point of maximum vorticity; the location of the latter in between the grid nodes is approximated with the second-order finite-difference scheme. The (unit) normal vector $\boldsymbol{n}_1$ to the pancake is defined as the eigenvector corresponding to the largest of the three eigenvalues $|\lambda_1| \geqslant |\lambda_2| \geqslant |\lambda_3|$ of the Hessian. The pancake thickness ℓ_1, as well as its lateral scales ℓ_2 and ℓ_3, can be estimated with the local second-order approximation as $\ell_i = \sqrt{2\omega^2_{max}/|\lambda_i|}$; see Agafontsev *et al.* (2015). Figure 1(*c*) shows these characteristic scales as functions of time. At late times, the pancake thickness ℓ_1 is exponentially decreasing, while the dimensions ℓ_2 and ℓ_3 do not change substantially, in agreement with the three-dimensional picture in figure 1(*b*). Thus, the pancake develops only one small scale corresponding to its transversal direction, and the vorticity growth is locally one-dimensional. The span-to-thickness ratio grows exponentially, reaching $\ell_2/\ell_1 \sim \ell_3/\ell_1 \gtrsim 100$ at the final time $t = 7.75$. The vorticity vector within the pancake structure is tangent to the pancake midplane and oriented roughly anti-parallel to the y-axis.

3. Exact solution of the Euler equations as a model for pancake evolution

Following the numerical results, we suggest an analytical model for the vorticity growth. Assuming that in Cartesian coordinates $\boldsymbol{a} = a_1\boldsymbol{n}_1 + a_2\boldsymbol{n}_2 + a_3\boldsymbol{n}_3$ the vorticity changes only along the a_1-axis and is oriented along the a_2-axis, we write

$$\boldsymbol{\omega}(\boldsymbol{a}, t) = \omega_2\boldsymbol{n}_2, \quad \omega_2 = \Omega(t) f'\left(\frac{a_1}{\ell_1(t)}\right), \tag{3.1}$$

where $\Omega(t)$ is the characteristic vorticity amplitude and $\ell_1(t)$ is the pancake thickness. The ansatz (3.1) contains a derivative (denoted by a prime) of an arbitrary function $f(\xi)$ taken at $\xi = a_1/\ell_1(t)$. One can check that (3.1) together with the velocity field

$$\boldsymbol{v}(\boldsymbol{a}, t) = -\Omega(t)\ell_1(t) f\left(\frac{a_1}{\ell_1(t)}\right)\boldsymbol{n}_3 + \begin{pmatrix} -\beta_1(t)a_1 \\ \beta_2(t)a_2 \\ \beta_3(t)a_3 \end{pmatrix} \tag{3.2}$$

represents an exact solution of the Euler equations (2.1), where $\beta_1(t)$, $\beta_2(t)$ and $\beta_3(t)$ are given by

$$\beta_1 = -\dot{\ell}_1/\ell_1, \quad \beta_2 = \dot{\Omega}/\Omega, \quad -\beta_1 + \beta_2 + \beta_3 = 0, \tag{3.3a–c}$$

with the dots denoting time derivatives. The velocity (3.2) is a superposition of the shear flow $-\Omega\ell_1 f(a_1/\ell_1)\boldsymbol{n}_3$ and the asymmetric irrotational straining flow $(-\beta_1 a_1, \beta_2 a_2, \beta_3 a_3)$, and satisfies the Euler equations $\dot{\boldsymbol{v}} + \boldsymbol{v}\cdot\boldsymbol{\nabla}\boldsymbol{v} = -\boldsymbol{\nabla}p$ with the pressure

$$p = p_0 + (\dot{\beta}_1 - \beta_1^2)\frac{a_1^2}{2} - (\dot{\beta}_2 + \beta_2^2)\frac{a_2^2}{2} - (\dot{\beta}_3 + \beta_3^2)\frac{a_3^2}{2}. \tag{3.4}$$

It should be noted that the pressure is determined entirely by the coefficients β_1, β_2 and β_3 of the straining flow. A uniform velocity field with an arbitrary time dependence $(0, v_{b2}(t), v_{b3}(t))$ can be added to (3.2). This field, describing a drift of the pancake structure, leads to the change of pressure as $p \to p - a_2(\beta_2 v_{b2} + \dot{v}_{b2}) - a_3(\beta_3 v_{b3} + \dot{v}_{b3})$.

The suggested solution is an essential generalization of the pancake model of Brachet *et al.* (1992); the latter is obtained as a special case with $\Omega = \ell_1^{-1} = \mathrm{e}^{t/T}$, $\beta_{1,2} = 1/T$, $\beta_3 = 0$. The solution (3.1)–(3.4) has infinite energy in $\mathbb{R}^3$ and allows for an arbitrary time dependence of $\Omega(t)$ and $\ell_1(t)$, in particular, the one leading to a finite-time blowup. In addition to an arbitrary function $f(\xi)$, the new solution is characterized by a single dimensionless parameter

$$\sigma = \frac{\beta_2 - \beta_3}{\beta_2 + \beta_3} = \frac{2\beta_2}{\beta_1} - 1, \tag{3.5}$$

describing the asymmetry of the straining flow in (3.2). In our numerical simulations, nearly exponential behaviour for $\Omega(t)$ (vorticity maximum) and $\ell_1(t)$ is observed, see figure 1(*a*,*c*), which corresponds to constant numbers for β_1, β_2 and β_3 in (3.3). Then, the asymmetry parameter defines the exponent in the power-law relation

$$\Omega(t) \propto \ell_1(t)^{-\zeta}, \quad \zeta = \frac{\beta_2}{\beta_1} = \frac{\sigma + 1}{2} \tag{3.6a,b}$$

between the vorticity amplitude and the pancake thickness. Consequently, in the transversal direction, the velocity has variation $\delta v_3 \propto \Omega \ell_1 \propto \ell_1^{1-\zeta}$ at the scale of the pancake thickness $\delta a_1 \sim \ell_1$, and this variation vanishes for $\zeta < 1$ (i.e. $\sigma < 1$) as $\ell_1 \to 0$.

The solution (3.1)–(3.4) can be extended for the Navier–Stokes equations with kinematic viscosity ν, if the function $f(\xi, t)$ changes with time as $f_t - (\nu/\ell_1^2) f_{\xi\xi} = 0$. The latter becomes the heat equation after a simple transformation of time, $\tau = \int \mathrm{d}t/\ell_1^2(t)$. For the axisymmetric straining flow with $\beta_2 = \beta_3 = \beta_1/2$, the suggested solution becomes the special case of the Lundgren stretched-spiral vortex; see Lundgren (1982). It should be noted that solutions of the Navier–Stokes equations in the form of stretched vortices embedded in a uniform straining flow were first studied by Burgers (1948); see also Prochazka & Pullin (1998), Pullin & Saffman (1998), Gibbon, Fokas & Doering (1999) and Maekawa (2009).

4. Comparison with the numerical simulations

In simulations, we define the local coordinate system (a_1, a_2, a_3) for the pancake structure in the following way. The origin is chosen at the point of the global vorticity maximum, where we also compute the pancake normal vector $\boldsymbol{n}_1$ of the a_1-axis, as described in § 2. According to the exact solution (3.1), the a_2-axis should be parallel to the vorticity vector $\boldsymbol{\omega}$. However, in simulations, the angle between $\boldsymbol{n}_1$ and $\boldsymbol{\omega}$ may differ from 90°. We checked that this difference, in fact, is tiny, reaching 0.02° at the final time. Thereby, we define the a_2-axis with the direction $\boldsymbol{n}_2 = c[\boldsymbol{\omega} - (\boldsymbol{\omega} \cdot \boldsymbol{n}_1)\boldsymbol{n}_1]$, where $(\boldsymbol{\omega} \cdot \boldsymbol{n}_1)\boldsymbol{n}_1$ is a small correction and the prefactor c is chosen such that $\|\boldsymbol{n}_2\| = 1$. Finally, the a_3-axis has the direction $\boldsymbol{n}_3 = \boldsymbol{n}_1 \times \boldsymbol{n}_2$. It should be noted that this coordinate system is computed at each moment of time, which is necessary to account for a possible drift of the whole structure. We choose the vorticity amplitude as the maximum vorticity, $\Omega = \omega_{max}$, and compute coefficients β_1, β_2 and β_3 according to (3.3).

In this section, we provide several numerical tests supporting the pancake model proposed in § 3. The first test is related to self-similarity of the transversal vorticity profile, which should be kept, according to (3.1), as

$$\omega_2/\omega_{max} = f'(\xi), \quad \xi = a_1/\ell_1. \tag{4.1}$$

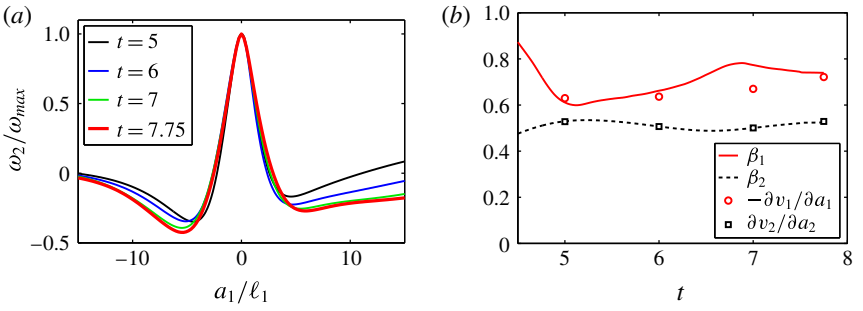

FIGURE 2. (*a*) Normalized vorticity component ω_2/ω_{max} as a function of $\xi = a_1/\ell_1$ at different times. (*b*) Comparison of the logarithmic derivatives $\beta_1 = -\dot{\ell}_1/\ell_1$ and $\beta_2 = \dot{\omega}_{max}/\omega_{max}$ with the velocity gradients $-\partial v_1/\partial a_1$ and $\partial v_2/\partial a_2$ computed at the global vorticity maximum; see (4.2). After prior computation of the time derivatives, ℓ_1 and ω_{max} are smoothed with the weighted local regression (lowess filter); see Cleveland, Devlin & Grosse (1988).

This is confirmed in figure 2(*a*), where the vorticity profile ω_2/ω_{max} along the a_1-axis is shown at different times. The self-similarity region grows with time in the ξ-coordinate, remaining finite in physical space, where it matches with the background flow. It should be noted that the function $f(\xi)$ may be arbitrary; in our simulations, different vorticity profiles are obtained for different pancakes and initial conditions.

For the analysis of the velocity field, one should take into account a drift of the pancake structure by a background flow with non-trivial time dependence. However, this difficulty can be avoided if we examine the velocity gradient, which for the pancake model solution (3.1)–(3.4) has the form

$$[\partial v_i/\partial a_j] = \begin{pmatrix} -\beta_1 & 0 & 0 \\ 0 & \beta_2 & 0 \\ -\omega_2 & 0 & \beta_3 \end{pmatrix}. \tag{4.2}$$

In figure 2(*b*), we compare at different times the logarithmic derivatives $\beta_1 = -\dot{\ell}_1/\ell_1$ and $\beta_2 = \dot{\omega}_{max}/\omega_{max}$ with the velocity gradients $-\partial v_1/\partial a_1$ and $\partial v_2/\partial a_2$ evaluated at the global vorticity maximum. One can see very good overall agreement, with a larger deviation for $-\partial v_1/\partial a_1$ at $t = 7$. This deviation can be attributed to the variation (up to 20 %) of the velocity derivative within the pancake thickness. At the final simulation time $t = 7.75$ and at the global vorticity maximum, the numerical velocity gradient is given by

$$[\partial v_i/\partial a_j]_{\boldsymbol{a}=0} = \begin{pmatrix} -0.72 & -0.04 & -0.03 \\ -0.11 & 0.53 & -0.09 \\ -18.42 & -0.04 & 0.19 \end{pmatrix}, \tag{4.3}$$

confirming that there is a single large (3, 1)-component, $\partial v_3/\partial a_1 \approx -\omega_{max}$. The diagonal components corresponding to the straining flow are in very good agreement with the coefficients $-\beta_1 = -0.74$, $\beta_2 = 0.53$ and $\beta_3 = 0.21$, while the remaining components, (1, 2), (1, 3), (2, 1), (2, 3) and (3, 2) corresponding to vanishing elements in (4.2) are small.

The previous tests confirmed that the pancake model solution agrees with the flow in the vicinity of the global vorticity maximum. However, this model cannot

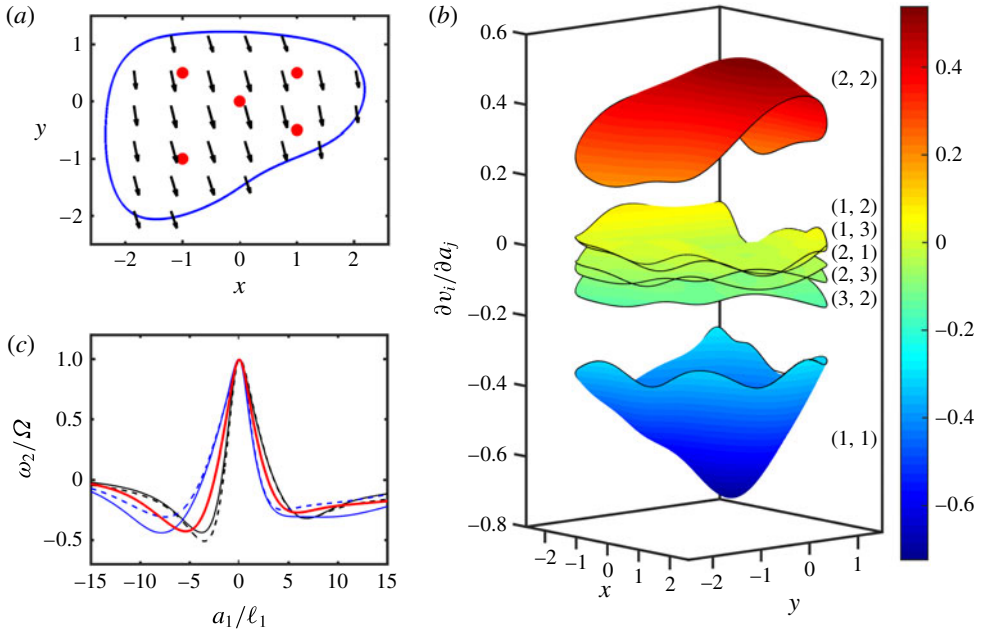

FIGURE 3. (*a*) Pancake midplane (vorticity above 70 % of the maximum value) in the projection to the (x, y)-plane. The arrows show projections of the vorticity vector, scaled by a factor of 0.025. The coordinates are shifted to place the vorticity maximum at the origin. (*b*) Velocity derivatives $\partial v_i/\partial a_j$ evaluated at different points of the pancake midplane; marked with (i, j). (*c*) Normalized vorticity profile ω_2/Ω in the direction perpendicular to the midplane, at five different points corresponding to the red dots in (*a*). The red line corresponding to the centre of the pancake is the same as in figure 2(*a*).

describe the whole region of high vorticity, since the pancake is not completely flat, with deviations from the plane $a_1 = 0$ much larger than the pancake thickness; see figure 1(*b*). Nevertheless, we can check whether the model approximates the pancake locally, at every nearly flat pancake segment. For this purpose, we consider the final time and isolate the principal part of the pancake with vorticity $\omega \geqslant 0.7\omega_{max}$; the isolated region is roughly parallel to the (x, y)-plane. Despite the fact that this region is very thin, $\ell_1 \sim 0.01$, its lateral dimensions are comparable to the size of the numerical box, as shown by the projection to the (x, y)-plane in figure 3(*a*). Within this region, we define the pancake midplane $z = z_m(x, y)$, chosen as points of maximum vorticity, $\max_z \omega$, for the given values of x and y. Then, at each point $\boldsymbol{r}_m = (x, y, z_m(x, y))$ of the midplane, we define the new local coordinates (a_1, a_2, a_3), using the first eigenvector of the Hessian matrix and the vorticity vector, as described above in this section. It should be noted that (x, y) serve as parameters in this representation, while the coordinates (a_1, a_2, a_3) explore the neighbourhood of $\boldsymbol{r}_m$.

First, we verified numerically that, within the pancake, the vorticity vector is tangent to the midplane and almost unidirectional. This is illustrated in figure 3(*a*), where projections to the (x, y)-plane of the vorticity vector are shown by arrows, which are scaled (multiplied by 0.025) to fit the plot. At several distant points on the midplane, we considered the vorticity profile ω_2/Ω as a function of a_1/ℓ_1, where $\Omega = \max_z \omega$ is the vorticity at the corresponding point on the midplane. At every point, a convergence similar to figure 2(*a*) is observed, showing that the vorticity profile changes with time

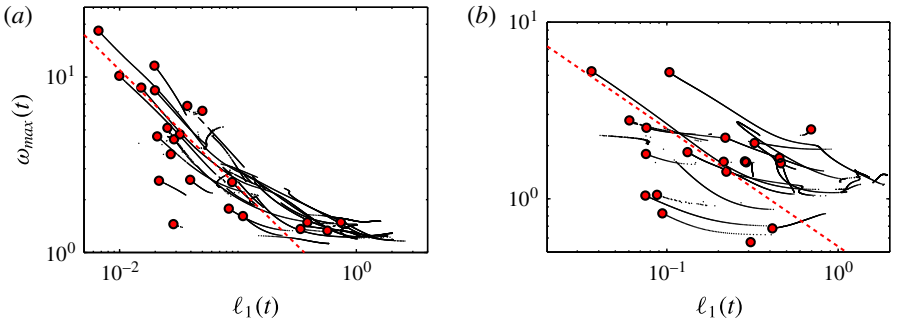

FIGURE 4. (*a*) Relation between the vorticity local maxima $\omega_{max}(t)$ and the respective characteristic lengths $\ell_1(t)$ during the evolution of the pancake structures. The lines represent the evolution of the maxima with increasing time, with the red dots corresponding to the final simulation time. The dashed red line indicates the power-law scaling $\omega_{max} \propto \ell_1^{-2/3}$. (*b*) The same graph for a different simulation with a generic initial condition and the final grid $1152 \times 972 \times 864$.

self-similarly according to (4.1); the convergence gets worse near the pancake border. The vorticity profile varies from point to point; this means that the function $f(\xi)$ of the model (3.1) changes along the pancake. The magnitude of this variation can be seen in figure 3(*c*), which presents the final-time vorticity profiles ω_2/Ω at five different points marked with red dots in panel (*a*) of the same figure. It should be noted that a specific form of $f(\xi)$ is not important in the exact solution (3.1)–(3.2). Thus, this function accounts for the local self-similarity only, while its variations along the pancake may be captured by a next-order correction to our model.

The structure of the gradient (4.2) is confirmed in figure 3(*b*) along the whole pancake midplane. The components (1, 2), (1, 3), (2, 1), (2, 3) and (3, 2) are concentrated in the middle of the figure: they are approximately one order of magnitude smaller than the diagonal components and more than two orders of magnitude smaller than the (3, 1)-component related to the vorticity. The large (3, 1)-component does not fit to the vertical range of the figure, but it is in excellent agreement with the vorticity, $\partial v_3/\partial a_1 \approx -\omega$, with the difference below 0.6 %. The diagonal components $\partial v_1/\partial a_1$ (blue) and $\partial v_2/\partial a_2$ (red) vary significantly along the midplane. We do not show $\partial v_3/\partial a_3$ due to its exact relation to (1, 1)- and (2, 2)-components, originating from incompressibility of the flow, $\operatorname{div} \boldsymbol{v} = 0$. With these observations, we confirm that, for every nearly flat pancake segment, the flow can be approximated by the pancake model solution suggested in § 3.

As was noticed in Agafontsev *et al.* (2015), at late times the pancakes develop according to the Kolmogorov-like power law

$$\omega_{max}(t) \sim \ell_1(t)^{-\zeta}, \quad \zeta \approx 2/3. \tag{4.4}$$

This tendency is clearly seen in figure 4(*a*), where all other local vorticity maxima are shown and the 2/3-slope is represented by the dashed line. We stress that the pancake model solution (3.1)–(3.4) allows for an arbitrary power-law exponent ζ. Thus, the universality of the asymptotic value $\zeta = 2/3$, which corresponds to the asymmetry parameter $\sigma = 1/3$ of the straining flow, goes beyond this solution. We think that restrictions on the power law may come from the non-local interactions of the pancakes and the background flow.

All of the results presented so far relate to the main pancake structure from the simulation with the I_1 initial condition. We confirmed that several other pancake structures, associated with some of the local vorticity maxima shown in figure 4(*a*), also agree with the pancake model solution. We performed a series of simulations in grids with a total number of nodes of 1024^3, starting from fully generic (large-scale) initial conditions. The regions of high vorticity, emerging from such initial flows, have arbitrary orientation, which does not allow us to use anisotropic grids effectively. Thereby, such simulations yield considerably smaller overall vorticity enhancement. However, these regions represent pancake-like structures developing close to the model solution (3.1)–(3.4), and the same relation (4.4) between the vorticity maximum and the pancake thickness is observed; see the example of one such simulation in figure 4(*b*).

5. Conclusions

We have studied high-vorticity regions developing in the 3D incompressible Euler equations from generic large-scale initial conditions. These regions represent pancake-like structures of increasing vorticity, which compress in a self-similar way in the transversal direction. Led by this observation, we proposed a novel exact solution of the 3D Euler equations, which describes this behaviour asymptotically. The proposed solution combines a shear flow aligned with an asymmetric irrotational straining flow, and is characterized by a single asymmetry parameter and an arbitrary transversal vorticity profile. It should be noted that a pancake structure is not completely flat, with deviations much larger than the pancake thickness. It is remarkable that the proposed analytical model describes locally every nearly flat pancake segment, while the model parameters may change from one segment to another. The latter may be captured in next-order corrections to our pancake model, which is an interesting topic for future studies. In simulations, we observe exponential evolution of the vorticity maximum and pancake thickness, with a Kolmogorov-like relation between the two, $\omega_{max}(t) \propto \ell_1(t)^{-2/3}$. This behaviour is not required by the suggested model, and presumably relates to non-local effects.

Acknowledgements

Simulations were performed at the Novosibirsk Supercomputer Center (NSU) and the Data Center of IMPA (Rio de Janeiro). The work of D.S.A. and E.A.K. was supported by the Russian Science Foundation (grant 14-22-00174). D.S.A. acknowledges the support from IMPA during visits to Brazil. A.A.M. was supported by the CNPq (grant 302351/2015-9) and the Program FAPERJ Pensa Rio (grant E-26/210.874/2014).

References

AGAFONTSEV, D. S., KUZNETSOV, E. A. & MAILYBAEV, A. A. 2015 Development of high vorticity structures in incompressible 3D Euler equations. *Phys. Fluids* **27**, 085102.

BRACHET, M. E., MENEGUZZI, M., VINCENT, A., POLITANO, H. & SULEM, P. L. 1992 Numerical evidence of smooth self-similar dynamics and possibility of subsequent collapse for three-dimensional ideal flows. *Phys. Fluids* A **4**, 2845–2854.

BURGERS, J. M. 1948 A mathematical model illustrating the theory of turbulence. *Adv. Appl. Mech.* **1**, 171–199.

BUSTAMANTE, M. D. & BRACHET, M. 2012 Interplay between the Beale–Kato–Majda theorem and the analyticity-strip method to investigate numerically the incompressible Euler singularity problem. *Phys. Rev.* E **86** (6), 066302.

CHAE, D. 2008 Incompressible Euler equations: the blow-up problem and related results. In *Handbook of Differential Equations: Evolutionary Equation* (ed. C. M. Dafermos & M. Pokorny), vol. 4, pp. 1–55. Elsevier.

CLEVELAND, W. S., DEVLIN, S. J. & GROSSE, E. 1988 Regression by local fitting: methods, properties, and computational algorithms. *J. Econom.* **37** (1), 87–114.

GIBBON, J. D. 2008 The three-dimensional Euler equations: where do we stand? *Physica* D **237** (14–17), 1894–1904.

GIBBON, J. D., FOKAS, A. S. & DOERING, C. R. 1999 Dynamically stretched vortices as solutions of the 3D Navier–Stokes equations. *Physica* D **132** (4), 497–510.

HOU, T. Y. 2009 Blow-up or no blow-up? a unified computational and analytic approach to 3D incompressible Euler and Navier–Stokes equations. *Acta Numerica* **18**, 277–346.

HOU, T. Y. & LI, R. 2007 Computing nearly singular solutions using pseudo-spectral methods. *J. Comput. Phys.* **226** (1), 379–397.

KERR, R. M. 2013 Bounds for Euler from vorticity moments and line divergence. *J. Fluid Mech.* **729**, R2.

LUNDGREN, T. S. 1982 Strained spiral vortex model for turbulent fine structure. *Phys. Fluids* **25**, 2193.

MAEKAWA, Y. 2009 On the existence of Burgers vortices for high Reynolds numbers. *J. Math. Anal. Appl.* **349** (1), 181–200.

MAJDA, A. J. & BERTOZZI, A. L. 2002 *Vorticity and Incompressible Flow*. Cambridge University Press.

OHKITANI, K. 2008 A geometrical study of 3D incompressible Euler flows with Clebsch potentials – a long-lived Euler flow and its power-law energy spectrum. *Physica* D **237** (14), 2020–2027.

PROCHAZKA, A. & PULLIN, D. I. 1998 Structure and stability of non-symmetric Burgers vortices. *J. Fluid Mech.* **363**, 199–228.

PULLIN, D. I. & SAFFMAN, P. G. 1998 Vortex dynamics in turbulence. *Annu. Rev. Fluid Mech.* **30** (1), 31–51.

PUMIR, A. & SIGGIA, E. 1990 Collapsing solutions to the 3-D Euler equations. *Phys. Fluids* A **2**, 220–241.